ELSEVIER

Journal of Alloys and Compounds 320 (2001) 308–319

Journal of ALLOYS AND COMPOUNDS

www.elsevier.com/locate/jallcom

Constitution, structural chemistry and magnetism in the ternary system Ce–Ag–Si ☆

Edgar Cordruwisch[a], Dariusz Kaczorowski[b], Peter Rogl[a,*], Adriana Saccone[c], Riccardo Ferro[c]

[a]*Institut für Physikalische Chemie der Universität Wien, A-1090 Wien, Währingerstraße 42, Austria*

[b]*W. Trzebiatowski Institute for Low Temperature and Structure Research, Polish Academy of Science, P-50-950 Wroclaw, P.O. Box 937, Poland*

[c]*Dipartimento di Chimica e Chimica Industriale, Università di Genova, Sezione di Chimica Inorganica e Metallurgica, Via Dodecaneso 31, I-16146 Genova, Italy*

Abstract

Phase relations were established for the Ce–Ag–Si system at 850°C by means of X-ray diffraction, light optical microscopy and quantitative electron probe microanalysis. Phase equilibria are characterised by the existence of extended solid solutions starting from the binaries: $Ce(Ag_xSi_{1-x})_{2-y}$ ($ThSi_2$-type), $Ce(Ag_{1-x}Si_x)_{1-y}$ (unknown structure type) and $Ce(Ag_{1-x}Si_x)_{2-y}$ (unknown structure type). Three ternary phases were found to exist, $CeAg_2Si_2$ ($ThCr_2Si_2$-type), $Ce(Ag_xSi_{1-x})_{2-y}$ (AlB_2-type) and the new ternary compound $CeAgSi_2$ with unknown structure type. Magnetic behaviour was studied from magnetic susceptibility and magnetisation measurements down to 1.7 K and employing magnetic fields up to 5 T. Soft ferromagnetism is observed for $CeAg_xSi_{2-x}$ (AlB_2-type) below 5 K. Alloys $Ce(Ag_xSi_{1-x})_{2-y}$ with $0.08<x_{Ag}<0.30$ ($ThSi_2$-type) encounter ferromagnetic order below 7 K. For $x_{Ag}=0.31$ the ferromagnetic interaction changes to antiferromagnetism with $T_N=5.7$ K. For $CeAgSi_2$ ferrimagnetic or canted antiferromagnetic order is indicated below 7 K.

Keywords: Ce–Ag–Si system; Phase equilibria; Ternary phases; Ferromagnetism

1. Introduction

Whereas binary interaction of the rare earth elements with silicon and silver is well known and leads to a series of binary compounds, information on the corresponding ternary alloying behaviour Ce–Ag–Si is still rather scarce [13,17]. The discovery of the heavy fermion superconductor $CeCu_2Si_2$ [8] has spurred some interest in the physical properties of its isotypic homologue $CeAg_2Si_2$ [12]. A search for AlB_2-type representatives identified the compound $Ce(Ag_{0.33}Si_{0.67})_2$ without any details of its physical properties [16]. For an early review on the Ce–Ag–Si system see [17].

In the framework of our general interest in strongly correlated electron systems and valence instabilities, a thorough investigation of the constitution of the Ce–Ag–Si system, the formation of ternary compounds and solutions, their crystal structures and physical properties became the subject of the present paper.

Our investigation was based on the binary boundary systems as given in [20]. Points of interest, however, were reinvestigated in the course of the present work. The crystallographic data for the binary boundary systems are summarised in Table 1.

2. Experimental techniques

The alloys, each with a total weight of 0.5 to 1 g were synthesised by repeated argon arc melting ingots of the elements of 99.9 mass% minimum purity. For homogenisation a part of the alloy buttons was vacuum sealed in quartz capillaries and annealed at 850°C or 700°C for up to 330 h prior to quenching in cold water. The samples prepared near the Ce–Ag binary were found to be very sensitive to moisture. Under normal conditions these ingots decayed within days after preparation and cutting into X-ray amorphous products. The preparation was therefore carried out in a glove box under a protective environment with less than 5 ppm O_2 and H_2O. X-ray powder data were obtained in the D5000 X-ray diffractometer from powders mounted on a glass support, sealed by kaptan foil in a specially designed argon filled measuring chamber.

☆Dedicated to Prof. Dr. Alan Prince, in memoriam.

*Corresponding author. Tel.: +431-427-752-456; fax: +431-427-795-24.

E-mail address: peter.franz.rogl@univie.ac.at (P. Rogl).

0925-8388/01/$ – see front matter
PII: S0925-8388(00)01474-2

Table 1
Crystallographic and magnetic data for the unary and binary boundary phases in the system Ce–Ag–Si

Phase	Pears. symb.	Space-group	Strukturbericht design.	Structure type	Lattice parameters in nm *a*	*b*	*c*	Spin order	$T_{ord.}$ [K]	θ_P [K]	μ_{eff} [μ_B]	Comments	Reference
Ag	cF4	$Fm\bar{3}m$	A1	Cu	0.40857	–	–					0 to ~0.05 at.% Ce; ≤961.93°C	[20]
δCe	cI2	$Im\bar{3}m$	A2	W	0.41200	–	–					798 to 726°C; 0 to ~2 at.%Ag	[20]
γCe	cF4	$Fm\bar{3}m$	A1	Cu	0.51610	–	–					726 to 61°C; 0 to ~2 at.%Ag	[20]
βCe	hP4	$P6_3/mmc$	A3′	αLa	0.36810	–	1.1857					61 to −177°C	[20]
αCe	cF4	$Fm\bar{3}m$	A1	Cu	0.48500	–	–					<−177°C	[20]
αSi	cF8	$Fd\bar{3}m$	A4	C (diam.)	0.54309	–	–					≤1414°C	[20]
Ce_5Si_3 [a]												≤1400°C	[20]
	tI32	$I4/mcm$	$D8_1$	Cr_5B_3	0.78860	–	1.373						[26]
					1.10100			AF	10	−50			[22]
Ce_3Si_2	tP10	$P4/mbm$	$D5_a$	U_3Si_2								≤1390°C	[20]
					0.77900	–	0.436						[26]
Ce_5Si_4	tP36	$P4_12_12$	...	Zr_5Si_4								≤1440°C	[20]
					0.79500	–	1.500						[26]
CeSi	oP8	$Pnma$	B27	FeB								≤1470°C	[20]
					0.82900	0.396	0.598						[26]
								AF	5.6				[25]
								IC	1.5				
$CeSi_{2-x}$	oI12	$Imma$	...	$GdSi_{2-x}$								≤1560°C	[20]
					0.41890	0.4123	1.3875					$x=0.5$	[26]
					0.41900	0.4135	1.3872					$x=0.3$	
$CeSi_{2-x}$	tI12	$I4_1/amd$	C_c	$ThSi_2$								≤1620°C	[20]
					0.41680	–	1.3850					$x=0.23$	[26]
					0.41910	–	1.3949					$x=0$	
								F	12.0			$x=0.3$	[24]
								F	12.0			$x=0.2$	[23]
								F	5.5	−70		$x=0.07$	[22]
								[b]				$x=0.05$	[23]
βCeAg		...	...	unknown	...	...	...					870 to 470°C	[15]
αCeAg	cP2	$Pm\bar{3}m$	B2	CsCl	0.37850	–	–					<470°C	[15]
								F	9	−26	2.59		[22]
									5.3				
$\gamma CeAg_2$	...	...	...	unknown	...	...	...					855 to 748°C	[15]
$\beta CeAg_2$	...	...	...	unknown	...	...	...					748 to 540°C	[15]
$\alpha CeAg_2$	oI12	$Imma$	...	KHg_2 ($CeCu_2$)	0.48000	0.7090	0.8205					<540°C	[15]
$Ce_{14}Ag_{51}$	hP68	$P6/m$	...	$Gd_{14}Ag_{51}$								≤1041°C	[15]
					1.27790	–	0.9420					21.5 at.%Ce	
					1.28830	–	0.9455					~25 at.%Ce	
Ce_2Ag_9	...	...	...	unknown	...	...	...					≤838°C	[14,28]

[a] Erroneously listed as W_5Si_3-type in [18]; [26] erroneously reported the Mn_5Si_3-type from [1]; [26] also erroneously cited [11].
[b] No magnetic ordering.

Light optical microscopy (LOM) on selected alloys which were polished and etched by standard methods, scanning electron microscopy and microprobe analyses based on energy dispersive X-ray spectroscopy (Si(Li) detector) were used to examine phase equilibria and equilibrium compositions. For quantitative EMPA the samples were analysed employing an acceleration voltage of 20 kV for a counting time of 100 s. X-ray energy spectra from the Ce–L_α, Ag–L_α and Si–K_α radiation were processed using the ZAF-4/FLS software package supplied by LINK SYSTEMS Ltd., UK. A peak from a cobalt standard was used by a calibration procedure in order to monitor beam current, gain and resolution of the spectrometer. Pure elements served as standards to carry out the deconvolution of overlapping peaks and background subtraction. Finally the X-ray intensities were corrected for ZAF effects using the TIMI program [4]. In fine-grained micro-structures only phases with a grain size larger than ~8 μm were used for measurement.

Precise lattice parameters and standard deviations were obtained by a least-squares refinement of room-temperature Guinier–Huber X-ray ($CuK_{\alpha1}$) powder data. 2θ values were evaluated by reading the films with a digital positiometer. 6 N germanium ($a_{Ge}=0.5657906$ nm) served as an internal standard. For quantitative refinement of the atom positions, X-ray intensities were recorded from a flat specimen in a Siemens D5000 automatic powder diffractometer (CuK_α). Full matrix–full profile Rietveld refinements were performed employing the FULLPROF program [21]. Magnetisation and dc-magnetic susceptibility measurements were performed on polycrystalline samples in the temperature interval 1.7–300 K and in applied magnetic fields up to 5 Tesla using a Quantum Design MPMS-5 SQUID magnetometer. Susceptibility data were fitted to the Curie–Weiss law $\chi = C/(T-\theta)$.

3. Results and discussion

3.1. The binary boundary systems

Data from literature were obtained from a retrospective search of chemical abstracts by critical screening. Phase diagrams of the binary boundary systems were essentially accepted in the version presented by [20]. Considerable confusion, however, exists for the crystallographic modifications of the compound Ce_5Si_3. Rare earth silicides RE_5Si_3 crystallise with tetragonal Cr_5B_3-type for La to Nd but with hexagonal Mn_5Si_3-type for Sm to Lu except Eu [5]. Ce_5Si_3 was listed erroneously as W_5Si_3-type in [18]. [26] erroneously reported for Ce_5Si_3 a Mn_5Si_3-type from [1], and furthermore erroneously cited [11] by mistake. The latter author claims the formation of a new structure-type (Ce_5Si_3 (II)-type) after reaction of RE_5Si_3-type compounds with carbon. There is, however, no doubt about the stability of the Cr_5B_3-type for Ce_5Si_3 as reported in [1–3,5,7]. Our investigation confirms the Cr_5B_3-type at 850°C. The crystallographic data of the binary boundary phases are summarised in Table 1.

3.2. Solid phases

Whereas most of the binary cerium silicides exhibit rather small mutual solubility for silver i.e. less than ~1 at.% Ag, there is a significant solubility of Ag in Ce_3Si_2 (~2 at.% Ag). Quantitative electron microscopy confirmed the existence of CeAg and $CeAg_2$. Some confusion in literature exists with respect to the proper structural modification of CeAg. According to our experimental data there seems to be no difference between high and low temperature structure of CeAg: CeAg crystallises with the cubic CsCl-type without any visible structural transformation at 470°C reported in [15]. The solubility of Si replacing Ag in the binary cerium–silver compounds decreases with the Ag-content from ~8 at.% Si in CeAg, ~3.5 at.% Si in $CeAg_2$ to ~1.5 at.% Si in $Ce_{14}Ag_{51}$. There is practically no solubility of Ce and Ag in Si. A listing of the crystallographic data of the ternary solutions and compounds is given in Table 2. Comparison of the lattice parameters of the binary compounds with the parameters obtained in the ternary is shown in Table 3 also including the results of quantitative EMPA.

The homogeneous region of nonstoichiometric $CeSi_{2-y}$ was reinvestigated. At lower Si content the existence of the $GdSi_2$-type phase (orthorhombic distortion of tetragonal $ThSi_2$-type) was confirmed. The $ThSi_2$-type phase joins at decreasing Si-deficiency without any observable two phase region. The extension of the homogeneity range of $CeSi_{2-y}$ at 850°C was found to be rather small ranging at 850°C from y≈0.14 (35 at.% Ce) to ≈0.30 (37 at.% Ce). A third phase with an unknown X-ray pattern was observed in some nonequilibrium samples but disappeared after prolonged heat treatment.

3.3. Ternary phases; formation and structural chemistry

The existence of the ternary compound with the stoichiometric composition $CeAg_2Si_2$ and with $ThCr_2Si_2$-type

Table 2
Crystallographic and magnetic data for ternary compounds in the system Ce–Ag–Si

Nominal composition	Phase [EMPA in at.%]	Pears. symb.	Space-group	Structure type	Lattice parameters in nm			Spin order	T_{ord} [K]	σ_s $[\mu_B]$[a]	θ_p [K]	μ_{eff} $[\mu_B]$	Comments	Ref.
					a	*b*	*c*							
	$CeAg_2Si_2$	tI10	*I4/mmm*	$ThCr_2Si_2$	0.4247	–	1.064						800°C	[6]
					0.425	–	1.066	AF	10				800°C	[12]
$Ce_{18}Ag_{42}Si_{40}$	[21.8–39.6–38.7]				0.42478(14)	–	1.06475(53)	AF	9.5	0.17	−7.1	2.40	850°C/16d	this work
$Ce_{25}Ag_{25}Si_{50}$	$CeAgSi_2$	...	...	...				F	6.5	2.9	−24.0	2.13	850°C/10d	this work
	$Ce(Ag_xSi_{1-x})_{2-y}$	hP3	*P6/mmm*	AlB_2	0.4270	–	0.4197						$x=0.33$, $y=0$	[16]
	$CeAg_{0.9}Si_{1.1}$				0.4240(2)		0.4203(3)						600°C/1000 h	[33]
$Ce_{33}Ag_{23}Si_{44}$	[33.7–23–43.3]				0.42394(29)	–	0.42348(26)	F	3.9	1.0	−3.5	2.48	850°C/10d; $x=0.34$, $y=0$	this work
$Ce_{34}Ag_5Si_{61}$	$Ce(Ag_xSi_{1-x})_{2-y}$	tI12	*I4₁/amd*	$ThSi_2$	0.42042(7)	–	1.40776(34)	AF	5.7	0.9	−3.8	2.32	850°C/13d; $x=0.08$, $y=0.06$	this work
$Ce_{34}Ag_5Si_{61}$					0.42028(10)	–	1.40644(32)	F	6.0	0.5	−46.9	2.39	850°C/13d; $x=0.08$, $y=0.06$	this work
$Ce_{35}Ag_{10}Si_{55}$					0.41916(22)	–	1.41962(72)	F	4.7	0.8	−7.9	2.40	850°C/10d; $x=0.15$, $y=0.14$	this work
$Ce_{34}Ag_{10}Si_{56}$					0.42131(16)	–	1.42804(53)	F	7.0	0.8	−12.2	2.39	850°C/13d; $x=0.15$, $y=0.06$	this work
$Ce_{34}Ag_{15}Si_{51}$					0.42200(15)	–	1.44213(44)	F	4.5	0.9	−9.9	2.53	850°C/13d; $x=0.20$, $y=0.06$	this work
$Ce_{34}Ag_{20}Si_{46}$	$Ce(Ag_xSi_{1-x})_{2-y}$	tI12	*I4₁/amd*	$ThSi_2$	0.42291(15)	–	1.46374(93)	F	5.0	0.5	−49.1	2.58	850°C/20d; $x=0.30$, $y=0.06$ with traces of CeSi	this work
$Ce_{30}Ag_{30}Si_{40}$	$Ce(Ag_xSi_{1-x})_{2-y}$ [34.3–19.9–45.8]	tI12	*I4₁/amd*	$ThSi_2$	0.42301(19)	–	1.46472(70)	AF	5.7	0.8	−7.5	2.40	850°C/10d; $x=0.31$, $y=0.22$ with traces of Ag	this work
$Ce_{33}Ag_{23}Si_{44}$	$Ce(Ag_xSi_{1-x})_{2-y}$	tI12	*I4₁/amd*	$ThSi_2$	0.42352(7)	–	1.46983(33)	F	5.5	0.4	−9.6	2.53	as cast; $x=0.35$, $y=0$	this work
	$CeAg_{1.12}Si_{0.88}$	tI12	*I4₁/amd*	$ThSi_2$	0.42346(2)	–	1.4712(1)						600°C/1000 h	[33]

[a] Saturation moment σ_S was measured at 1.7 K.

Table 3
Crystallographic and microanalysis data of alloys Ce–Ag–Si

Nominal alloy comp in at% Ce–Ag–Si	Heat treat.	Phase analysis	Space group	Structure type	Lattice parameters in nm			Microprobe analysis[a] in at.%		
					a	*b*	*c*	Ce	Ag	Si
$Ce_{20}Si_{80}$	850°C/10d	$Ce_{14}Ag_{51}$	*P6/m*	$Gd_{14}Ag_{51}$	1.28910(28)	–	0.95054(32)			
$Ce_{25}Ag_{75}$	850°C/10d	$Ce_{14}Ag_{51}$	*P6/m*	$Gd_{14}Ag_{51}$	1.28821(24)	–	0.94905(77)			
$Ce_{35}Si_{65}$	850°C/10d	Si	$Fd\bar{3}m$	C (diam.)	0.54335(11)	–				
		$CeSi_{2-x}$	$I4_1/amd$	$ThSi_2$	0.41854(22)	–	1.38654(22)	36.3	0.0	63.8
$Ce_{36}Si_{64}$	850°C/13d	$CeSi_{2-x}$	*Imma*	$GdSi_2$	0.41813(8)	0.41662(16)	1.38574(29)	36.8	0.0	63.2
$Ce_{40}Si_{60}$	850°C/10d	$CeSi_{2-x}$	*Imma*	$GdSi_2$	0.41928(11)	0.41150(10)	1.39179(53)	37.0	0.0	63.0
		CeSi	*Pnma*	FeB	0.829880(11)	0.39709(16)	0.59684(80)	55.9	0.0	44.1
$Ce_{56}Si_{44}$	850°C/10d	CeSi	*Pnma*	FeB	0.83023(79)	0.39700(11)	0.59489(35)			
		Ce_5Si_4	$P4_12_12$	Zr_5Si_4	0.79497(16)	–	1.50765(68)			
$Ce_{62.5}Si_{37.5}$	850°C/10d	Ce_3Si_2	*P4/mbm*	U_3Si_2	0.78067(13)	–	0.43335(16)			
		Ce_5Si_3	*I4/mcm*	Cr_5B_3	0.79189(61)	–	1.38305(80)			
$Ce_{58}Ag_{20}Si_{26}$	850°C/10d	Ce_3Si_2	*P4/mbm*	U_3Si_2	0.78175(11)	–	0.43434(19)	62.5	1.3	36.2
		CeAg				–		52.7	39.4	8.3
$Ce_{43}Ag_{32}Si_{26}$	850°C/10d	CeSi	*Pnma*	FeB	0.83114(56)	0.3964(30)	0.59646(56)	50.1	1.0	48.9
		$CeAg_2$				–		35.4	61.3	3.4
$Ce_{37}Ag_{31}Si_{33}$	850°C/10d	$CeAg_xSi_{2-x}$	*P6/mmm*	AlB_2	0.42745(7)	–	0.42004(11)			
		CeSi	*Pnma*	FeB	0.83020(34)	0.39645(10)	0.59642(37)			
		$Ce_{14}Ag_{51}$	*P6/m*	$Gd_{14}Ag_{51}$	1.28973(15)	–	0.94950(9)			
$Ce_{37}Ag_{29}Si_{34}$	850°C/10d	$CeAg_xSi_{2-x}$	*P6/mmm*	AlB_2	0.42772(5)	–	0.41960(6)	33.9	23.1	43.0
		CeSi	*Pnma*	FeB	0.82940(105)	0.39663(12)	0.59625(41)	–		
		$Ce_{14}Ag_{51}$	*P6/m*	$Gd_{14}Ag_{51}$	1.28932(78)	–	0.93704(60)	22.5	76.1	1.4
$Ce_{18}Ag_{42}Si_{40}$	850°C/10d	$CeAgSi_{2-x}$	*I4/mmm*	$ThCr_2Si_2$	0.42500(26)	–	1.06601(48)	21.2	39.6	39.2
		Si	$Fd\bar{3}m$	C (diam.)	0.54258(26)	–	–	–		
		Ag	$Fm\bar{3}m$	Cu	traces			0.4	98.8	0.8
$Ce_{52}Ag_3Si_{45}$	850°C/10d	CeSi	*Pnma*	FeB	0.82900(94)	0.39784(19)	0.59641(68)			
		Ce_5Si_4	$P4_12_12$	Zr_5Si_4	0.79541(57)	–	1.50350(94)			
$Ce_{32}Ag_{48}Si_{20}$	850°C/10d	$Ce_{14}Ag_{51}$	*P6/m*	$Gd_{14}Ag_{51}$	1.28912(50)	–	0.94911(75)			
		$CeAg_xSi_{2-x}$	*P6/mmm*	AlB_2	0.42724(40)	–	0.41931(59)			
		CeSi	*Pnma*	FeB	0.82899(68)	0.39639(27)	0.59633(97)			
$Ce_{20}Ag_{20}Si_{60}$	as cast	Si	$Fd\bar{3}m$	C (diam.)	0.54319(48)	–	–	0.2	0.2	99.6
		$Ce(Ag,Si)_{2-x}$	$I4_1/amd$	$ThSi_2$	0.42142(27)	–	1.41773(81)	34.8	7.4	57.9
		$CeAg_2Si_2$	*I4/mmm*	$ThCr_2Si_2$	0.42457(23)	fine grains	1.06371(75)	25.0	29.9	45.1
		$CeAgSi_2$				fine peritec.		–		
	850°C/10d	Si	$Fd\bar{3}m$	C (diam.)				–	–	100.0
		$Ce(Ag,Si)_{2-x}$	$I4_1/amd$	$ThSi_2$	0.42219(25)	–	1.42194(64)	32.6	7.6	59.8
		$CeAgSi_2$						25.8	25.0	49.3
$Ce_{40}Ag_{20}Si_{40}$	850°C/10d	CeSi	*Pnma*	FeB	0.83022(90)	0.39683(13)	0.59669(42)			
		$CeAg_xSi_{2-x}$	*P6/mmm*	AlB_2	0.42740(70)	–	0.42001(94)			
$Ce_{26}Ag_{32}Si_{42}$	850°C/10d	$Ce(Ag,Si)_{2-x}$	$I4_1/amd$	$ThSi_2$	0.42225(27)	–	1.44607(56)	34.1	13.3	52.6
		$CeAg_2Si_2$	*I4/mmm*	$ThCr_2Si_2$	0.42575(4)	–	1.06184(34)	21.8	40.1	38.1
		Ag	$Fm\bar{3}m$	Cu	small amount			0.4	99.4	0.2
$Ce_{50}Ag_8Si_{42}$	850°C/10d	CeSi	*Pnma*	FeB	0.82956(42)	0.39804(9)	0.59655(29)	51.5	1.7	46.8
		Ce_5Si_4	$P4_12_12$	Zr_5Si_4	0.79830(50)	–	1.50686(89)	–		
		$CeAg_2$			small amount			35.3	62.2	2.6
$Ce_{55}Ag_5Si_{40}$	850°C/10d	Ce_3Si_2	*P4/mbm*	U_3Si_2	0.78131(35)	–	0.43460(18)	58.4	1.0	40.6
		Ce_5Si_4	$P4_12_12$	Zr_5Si_4	0.79507(62)	–	1.50527(92)	55.6	1.4	43.1
		$CeAg_2$			traces			–		
$Ce_{60}Ag_5Si_{35}$	850°C/10d	Ce_3Si_2	*P4/mbm*	U_3Si_2	0.78182(8)	–	0.43409(10)	62.3	1.8	35.6
		CeAg						52.1	40.5	7.6
$Ce_{39}Ag_{15}Si_{46}$	850°C/10d	$CeAg_xSi_{2-x}$	*P6/mnm*	AlB_2	0.42819(21)	–	0.42702(19)			
		CeSi	*Pnma*	FeB	0.82964(34)	0.39662(18)	0.59694(57)			
$Ce_{40}Ag_5Si_{55}$	850°C/10d	CeSi	*Pnma*	FeB	0.82876(44)	0.39718(16)	0.59695(54)			
		$Ce(Ag,Si)_{2-x}$	$I4_1/amd$	$ThSi_2$	0.41890(25)	–	1.42034(44)			
$Ce_{25}Ag_5Si_{70}$	850°C/10d	Si	$Fd\bar{3}m$	C (diam.)	0.54278(13)	–	–	1.5	0.3	98.2
		$Ce(Ag,Si)_{2-x}$	$I4_1/amd$	$ThSi_2$	0.42156(5)	–	1.41503(56)	34.4	6.4	59.2
$Ce_{15}Ag_{70}Si_{15}$	850°C/10d	Ag	$Fm\bar{3}m$	Cu	0.40918(27)	–	–			
		$Ce(Ag,Si)_{2-x}$	$I4_1/amd$	$ThSi_2$	0.42309(5)	–	1.46322(45)			

Table 3. Continued

Nominal alloy comp in at% Ce–Ag–Si	Heat treat.	Phase analysis	Space group	Structure type	Lattice parameters in nm			Microprobe analysis[a] in at.%		
					a	*b*	*c*	Ce	Ag	Si
$Ce_{20}Ag_{30}Si_{50}$	850°C/10d	Si	$Fd\bar{3}m$	C (diam.)	0.54245(32)	–	–	0.4	0.7	98.9
		$CeAg_2Si_2$	$I4_1/mmm$	$ThCr_2Si_2$	0.42486(14)	–	1.06549(95)	22.3	37.9	39.8
		$CeAgSi_2$						26.2	27.4	45.9
$Ce_{35}Ag_{15}Si_{50}$	850°C/10d	CeSi	*Pnma*	FeB	0.83139(67)	0.39682(26)	0.59729(26)			
		$Ce(Ag,Si)_{2-x}$	$I4_1/amd$	$ThSi_2$	0.42253(11)	–	1.44629(38)			
$Ce_{19}Ag_{26}Si_{55}$	850°C/10d	Si	$Fd\bar{3}m$	C(diam.)	0.54278(11)	–	–			
		$CeAg_2Si_2$	$I4/mmm$	$ThCr_2Si_2$	0.42498(23)	–	1.06599(60)			
		$CeAgSi_2$								
$Ce_{26}Ag_{16}Si_{57}$	850°C/10d	Si	$Fd\bar{3}m$	C (diam.)	0.54311(4)	–	–			
		$Ce(Ag,Si)_{2-x}$	$I4_1/amd$	$ThSi_2$	0.42175(9)	–	1.41756(37)			
		$CeAg_2Si_2$	$I4/mmm$	$ThCr_2Si_2$	0.42533(15)	–	1.06461(49)			
		$CeAgSi_2$								
	850°C/10d	Si	$Fd\bar{3}m$	C (diam.)	0.54242(2)	–	–			
		$Ce(Ag,Si)_{2-x}$	$I4_1/amd$	$ThSi_2$	0.42166(5)		1.41182(62)			
		$CeAgSi_2$								
$Ce_{27}Ag_{36}Si_{36}$	850°C/10d	$Ce(Ag,Si)_{2-x}$	$I4_1/amd$	$ThSi_2$	0.42285(11)	–	1.46441(59)			
		Ag	$Fm\bar{3}m$	Cu	0.40931(25)	–	–			
$Ce_{40}Ag_{10}Si_{50}$	850°C/10d	CeSi	*Pnma*	FeB	0.83021(32)	0.39674(8)	0.59687(26)			
		$Ce(Ag,Si)_{2-x}$	$I4_1/amd$	$ThSi_2$	0.42239(18)	–	1.44451(80)			
$Ce_{25}Ag_{28}Si_{47}$	850°C/33d	$Ce(Ag,Si)_{2-x}$	$I4_1/amd$	$ThSi_2$	0.42166(15)	–	1.41859(71)	33.9	11.1	55.0
		$CeAgSi_2$						–		
		$CeAg_2Si_2$	$I4/mmm$	$ThCr_2Si_2$				21.4	38.7	39.9
$Ce_{25}Ag_{31}Si_{44}$	850°C/10d	$Ce(Ag,Si)_{2-x}$	$I4_1/amd$	$ThSi_2$	0.42122(32)	–	1.44758(67)	34.3	15.3	50.3
		$CeAg_2Si_2$	$I4/mmm$	$ThCr_2Si_2$	0.42503(18)	–	1.06434(47)	20.9	38.3	40.8
$Ce_{36}Ag_{22}Si_{42}$	850°C/10d	CeSi	*Pnma*	FeB	0.82930(60)	0.39659(26)	0.59650(80)	–		
		$Ce(Ag,Si)_{2-x}$	$I4_1/amd$	$ThSi_2$	0.42379(25)	–	1.46483(60)	–		
		$CeAg_xSi_{2-x}$	$P6/mmm$	AlB_2	0.42716(20)	–	0.41892(24)	34.7	24.1	41.3
		$Ce_{14}Ag_{51}$	$P6/m$	$Gd_{14}Ag_{51}$				21.8	77.3	0.9
$Ce_{39}Ag_{19}Si_{42}$	850°C/10d	CeSi	*Pnma*	FeB	0.82902(68)	0.39640(15)	0.59647(71)	51.2	0.4	48.4
		$CeAg_xSi_{2-x}$	$P6/mmm$	AlB_2	0.42761(23)	–	0.41965(13)	34.7	24.6	40.8
		$Ce_{14}Ag_{51}$	$P6/m$	$Gd_{14}Ag_{51}$				21.2	78.1	0.8
$Ce_{38}Ag_6Si_{56}$	850°C/30d	CeSi	*Pnma*	FeB	0.82863(56)	0.39609(16)	0.59563(38)			
		$Ce(Ag,Si)_{2-x}$	$I4_1/amd$	$ThSi_2$	0.4 1750(9)	–	1.40659(56)			
$Ce_{38}Ag_{12}Si_{50}$	850°C/30d	CeSi	*Pnma*	FeB	0.83008(36)	0.39665(9)	0.59644(42)			
		$Ce(Ag,Si)_{2-x}$	*Imma*	$GdSi_2$	0.42431(35)	0.42223(37)	1.44869(81)			
$Ce_{37}Ag_5,Si_{58}$	850°C/13d	CeSi	*Pnma*	FeB	0.83399(26)	0.39716(5)	0.59736(16)			
		$Ce(Ag,Si)_{2-x}$	$I4_1/amd$	$ThSi_2$	0.42048(34)	–	1.40882(82)			
$Ce_{25}Ag_{24},Si_{51}$	850°C/10d	$CeAgSi_2$						26.0	25.1	48.9
		$Ce(Ag,Si)_{2-x}$	$I4_1amd$	$ThSi_2$	traces			33.6	9.4	57.0

[a] Phase regions measured only if larger than 8 μm.

was confirmed (see Tables 2 and 3). We furthermore confirm a ternary phase with the AlB_2-type and with a small range of homogeneity $Ce(Si_{1-x}Ag_x)_{2-y}$ ($0.35 \leq x \leq 0.4$ and $y \approx 0$). A new ternary phase was found with the composition $CeAgSi_2$.

Starting from binary $CeSi_{2-y}$ ($0.14 \leq y \leq 0.30$), $Ce(Si_{1-x}Ag_x)_{2-y}$ with the defect $ThSi_2$-type forms a rather extended solution, in which up to about 20 at.% Ag can be substituted for Si at 850°C. With increasing Ag-contents the solid solution approaches the ideal stoichiometry $y=0$ at $x \approx 0.35$.The solid solution with the $ThSi_2$-type seems to melt congruently. As-cast samples, however, revealed a further extension into the ternary beyond the limit observed at 850°C. After annealing at 850°C these alloys transformed to the AlB_2-phase mentioned above. X-ray and LOM observations were unable to conclusively decide weather a two-phase field or a second order transformation exists for the two structure types, which are structurally closely related i.e. their crystal structures may be transformed into each other via a simple shift operation [9]. Although the $GdSi_{2-x}$-type is easily recognised in the Ce–Si binary at the Ce-rich boundary of the disilicide, there is no clear observation of the $GdSi_{2-x}$-type along the Ce-rich boundary of the ternary solid solution $Ce(Si_{1-x}Ag_x)_{2-y}$. Except for some cases we mostly observe a two-phase region between CeSi and the $ThSi_2$-type. This feature may, however, be related to the exceedingly low difference in free energy between the two closely related structure types of which the $ThSi_2$-type is the one with the higher (and congruent) melting temperature.

Systematic of the crystal structure of $ThCr_2Si_2$ was described in [27] and the physical (magnetical) behaviour by [19]. The unit cell may be described as a stacking of infinite layers of interconnected tetragonal $SiCr_4$ pyramids parallel to (001) with a layer of Ce between these pyramids. Ag-atoms are tetrahedrally surrounded by four Si-atoms; Si in turn has four Ag-neighbours and one Si-neighbour which altogether form a tetragonal pyramid. The Ag-position enables atoms to be placed in the structure and is surrounded by at least eight nearest neighbours of Ag or Si depending on the values of the free parameters.

3.3.1. Refinement of the solid solution $Ce(Ag_xSi_{1-x})_{2-y}$ with $ThSi_2$-type

From a general description of the systematic of the $ThSi_2$-type [27] we observe a general trend for transition metals to replace Si-atoms and/or to fill the existing voids in the Si-sublattice of rare earth disilicides. In $CeSi_{2-y}$ the Ag-atoms merely replace silicon thereby leaving the Si-defect virtually unchanged for $Ce(Ag_xSi_{1-x})_{2-y}$ for lower values of x. For higher Ag-concentrations the solution gradually reduces the defect reaching the ideal stoichiometry at $x=0.35$, $y=0$. As silver atoms are considerably larger than silicon atoms, Si/Ag substitution infers a positive volume change which is also reflected in the variation of the cell dimensions as a function of Ag-content (Fig. 1). Within the scatter of the experimental data the change of the unit cell dimensions and of the volume is linear and follows Vegard's rule up to the maximum Ag-content of $x=0.35$ at 850°C.

With respect to a possible (partial) ordering of Ag/Si atoms in terms of lower symmetry but ordered LaPtSi-type [10], the X-ray powder intensities of several selected alloy compositions within the solid solution range were used for quantitative Rietveld analyses. The results of refinement are presented in Table 4 and in all cases confirm the crystallographic symmetry and isotypism with the $ThSi_2$-type i.e. a random distribution of Ag/Si-atoms in the lattice. Occupation factors were refined and for all compositions studied correspond to the EMPA-data or nominal compositions. Due to the usually strong correlation with (isotropic) temperature factors B_j, the occupancies were kept fixed in the final runs to refine the B_j values. The interatomic distances merely reflect weak Ce–Ce interactions but close (Ag,Si)–(Ag,Si) contacts. The defects appear statistically distributed throughout the three-dimensional Ag/Si-network.

3.3.2. Refinement of $Ce(Ag_xSi_{1-x})_{2-y}$ with AlB_2-type

The formation of the AlB_2-type close to the composition $Ce(Ag_{0.33}Si_{0.67})_{2-y}$ ($y \approx 0$) suggests statistical occupation of (Si,Ag) atoms in the B-sites of AlB_2-type. In order to check on the possibility of partial atom order in a lower symmetry atom arrangement of LiBaSi-type, Rietveld analyses were performed on two selected compositions. For both cases better agreement factors indicate random occupation of Ag/Si-atoms in AlB_2-type symmetry. For details of the calculation see results in Table 4.

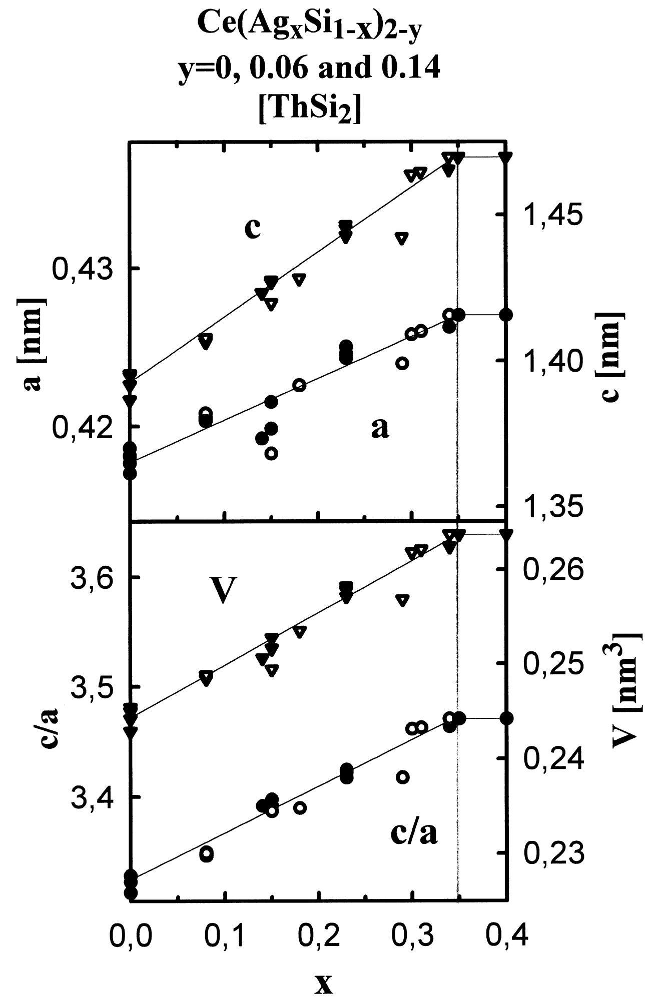

Fig. 1. Variation of lattice parameters versus Si/Ag substitution in the ternary solid solution $Ce(Ag_xSi_{1-x})_{2-y}$ [$ThSi_2$-type] (alloys quenched from 850°C). Open symbols indicate the magnetically characterised samples.

3.4. Isothermal section

Fig. 2 presents the phase equilibria as derived for 850°C based on X-ray diffraction, LOM and quantitative EMP-analyses. Crystallographic data evaluated by X-ray investigation and EMPA results are shown in Table 3. Phase equilibria are characterised by the rather large solid solution $Ce(Ag_xSi_{1-x})_{2-y}$ ($ThSi_2$-type and AlB_2-type). The observed tie-lines connecting the binary cerium silicides with Ag or the binary cerium silver compounds and solutions, respectively, indicate a relatively high thermodynamic stability of the equilibrium pairs: $ThSi_2$-

Table 4
Structural data for compounds $Ce(Ag_xSi_{1-x})_{2-y}$, quenched from 850°C[a]

Compound[b]	$Ce(Ag_{0.32}Si_{0.68})_{1.79}$	$Ce(Ag_{0.33}Si_{0.67})_2$	$Ce(Ag_{0.15}Si_{0.85})_{1.94}$	$Ce(Ag_{0.3}Si_{0.7})_{1.94}$	$Ce(Ag_{0.35}Si_{0.65})_2$
Number of reflections in refinement	52	60	109	116	117
Number of variables in refinement	25	14	19	24	22
Residual values:					
$R_e=\{(N-P+C)/\Sigma\omega_i Y_i^2(\text{obs})\}^{1/2}$	0.086	0.070	0.065	0.064	0.073
$\chi^2=\{R_P/R_e\}_2$	0.101	0.093	0.052	0.055	0.046
$R_P=\Sigma\|Y_i(\text{obs})-(1/c)Y_i(\text{calc})\|/\Sigma Y_i(\text{obs})$	0.183	0.168	0.111	0.113	0.113
$R_{wP}=[\Sigma w_i\|Y_i(\text{obs})-(1/c)Y_i(\text{calc})\|^2/\Sigma w_i\|Y_i(\text{obs})\|^2]^{1/2}$	0.275	0.216	0.148	0.151	0.140
$R_F=\Sigma\|[I_i(\text{obs})]^{1/2}-[I_i(\text{calc})]^{1/2}\|/\Sigma[I_i(\text{obs})]^{1/2}$	0.058	0.047	0.036	0.032	0.030
$R_I=\Sigma\|I_i(\text{obs})-(1/c)I_i(\text{calc})\|/\Sigma\|I_i(\text{obs})\|$	0.084	0.031	0.051	0.049	0.053
Preferred orientation coeff. for [*hkl*]	0.11(1), [101]	0.13(2), [101]	−0.07(1), [112]	−0.08(1), [112]	−0.13(1), [112]
Structure type–Space group	AlB_2–*P6/mmm*	AlB_2–*P6/mmm*	$ThSi_2$–$I4_1/amd$	$ThSi_2$–$I4_1/amd$	$ThSi_2$–$I4_1/amd$
Lattice parameters (in nm)[c]	*a* = 0.42732(5)	*a* = 0.42394(29)	*a* = 0.42131(16)	*a* = 0.42291(15)	*a* = 0.42352(7)
	c = 0.42012(14)	*c* = 0.42348(26)	*c* = 1.42804(53)	*c* = 1.46374(93)	*c* = 1.46983(33)
Atom parameters:					
atomic site for Ce-atom	1*a* (0,0,0)	1*a* (0,0,0)	4*a* (0,3/4,1/8)	4*a* (0,3/4,1/8)	4*a* (0,3/4,1/8)
Occupation	1	1	1	1	1
B in 10^{-2} nm^2	0.9(1)	0.27(4)	2.0(1)	1.4(1)	1.6(1)
atomic site for (Ag, Si)-atom	2*d* (1/3,2/3,1/2)	2*d* (1/3,2/3,1/2)	8*e* (0,1/4,0.2917(2))	8*e* (0,1/4,0.2921(2))	8*e* (0,1/4,0.2954(2))
Occupation	0.29(1)Ag + 0.61Si	0.33(1)Ag + 0.67(2)Si	0.15(1)Ag + 0.85(1)Si	0.29(1)Ag + 0.71(1)Si	0.35(2)Ag + 0.65(1)Si
B in 10^{-2} nm^2	1.5(2)	1.17(6)	2.2(1)	1.2(1)	1.6(1)
Interatomic distances/Central atom; standard deviations generally are smaller than < 0.0005 nm					
Ce	12 (Ag)–0.3240	12 (Ag)–0.3236	4 (Ag,Si)–0.3179	8 (Ag,Si)–0.3227	8 (Ag,Si)–0.3234
			8 (Ag,Si)–0.3208	4 (Ag,Si)–0.3233	4 (Ag,Si)–0.3244
			4 Ce–0.4145	4 Ce–0.4226	4 Ce–0.4243
(Ag, Si)	3 (Ag)–0.2467	3 (Ag)–0.2448	1 (Ag,Si)–0.2379	1 (Ag,Si)–0.2429	1 (Ag,Si)–0.2425
	6 (Ce)–0.3240	6 (Ce)–0.3236	2 (Ag,Si)–0.2420	2 (Ag,Si)–0.2448	2 (Ag,Si)–0.2456
			2 Ce–0.3179	4 Ce–0.3227	4 Ce–0.3233
			4 Ce–0.3208	2 Ce–0.3233	2 Ce–0.3242
Secondary Phase–Space group	$Ce(Ag_xSi_{1-x})_{2-y}$–$I4_1/amd$			CeSi–*Pnma*	$CeAg_xSi_{2-x}$–*P6/mmm*
Lattice parameters (in nm):	*a* = 0.42431(14)			*a* = 0.85865(26)	*a* = 0.42746(4)
	c = 1.4028(164)			b = 0.39633(11)	*c* = 0.41989(8)
				c = 0.59116(21)	

[a] Data collection from flat powder specimen–Siemens D5000; CuK_α-radiation; Theta range: $20° \leq 2\theta \leq 110°$.
[b] Composition determined from EMPA.
[c] Determined from Guinier–Huber X-ray film data.

type and AlB_2-type solution plus silver. This particular feature is documented in the micrograph of the as-cast and annealed alloy of $Ce_{26}Ag_{32}Si_{42}$ in Fig. 3.

The new compound $CeAgSi_2$ forms incongruently from the melt and thus can only be obtained in single phase form after prolonged heat treatment at elevated temperatures (900 to 1000°C). From the analysis of the micrographs of the as-cast and annealed alloy $CeAgSi_2$ (Fig. 4), the new compound $CeAgSi_2$ seems to form as needles in the interaction zone of a Ag-rich liquid around large primary crystals $Ce(Ag_xSi_{1-x})_{2-y}$ ($Ce_{33}Ag_{11}Si_{56}$ with $ThSi_2$-type). After 240 h of annealing at 850°C non-equilibrium still persists although the amount of $CeAgSi_2$ is increased together with $CeAg_2Si_2$.

Contrary to the system Ce–Ag–Ge, reported recently [29], corresponding compounds '$Ce_3Ag_4Si_4$, $Ce_4Ag_3Si_3$ and $Ce_6Ag_5Si_9$' were not observed. Similarly there is no indication for a corresponding compound 'Ce_2AgSi_6' in the range between 600 to 850°C.

3.5. Magnetic behaviour

The magnetic behaviour of the ternary Ce–Ag–Si alloys is summarised in Figs. 5–14 and in Tables 2–4. In the following the alloys will be treated individually as a function of their structure type.

$Ce(Ag_xSi_{1-x})_2$ (AlB_2–type): For $x_{Ag} = 0.34$ ferromagnetic order is observed below 3.9 K (see Fig. 5 and Table 2). Field dependency of the magnetisation without any hysteresis indicates soft ferromagnetism with $\sigma(5T) = 1.0$ μ_B at 1.7 K.

$Ce(Ag_xSi_{1-x})_{2-y}$ ($ThSi_{2-y}$–type): (see Figs. 6–12 and Table 2) According to [24], long range magnetic order

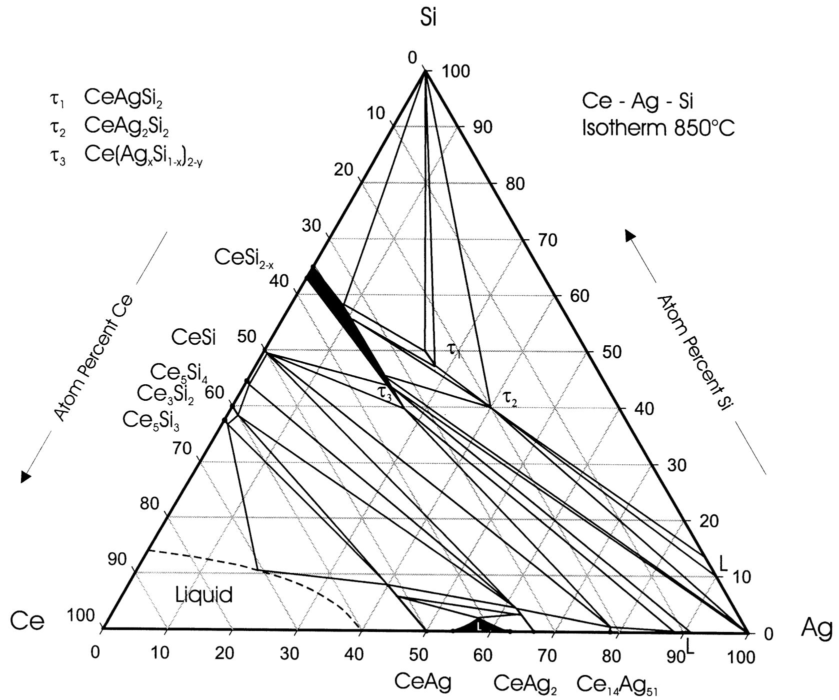

Fig. 2. The system Ce–Ag–Si, isothermal section at 850°C.

appears in binary $CeSi_{2-y}$ only for $y>0.2$. Yet, as shown in Figs. 6–8, a replacement of Si by Ag in the range $0.08<x_{Ag}<0.30$ induces ferromagnetism already for $y=0.06$. The Curie temperatures found for these alloys are in the range 4.5–7 K, and the saturation magnetic moment recorded at 1.7 K and 5 T is below 0.9 μ_B (see Figs. 11 and 12). On changing y ferromagnetism prevails with only minor variation of T_C but significant reduction of σ_s as observed for the alloy with $x_{Ag}=0.35$ and $y=0$ (Fig. 9). As displayed in Fig. 10, for $x_{Ag}=0.31$, $y=0.22$ the ferromagnetic interaction changes to antiferromagnetism with $T_N=5.7$ K. It is interesting to note, that an in-

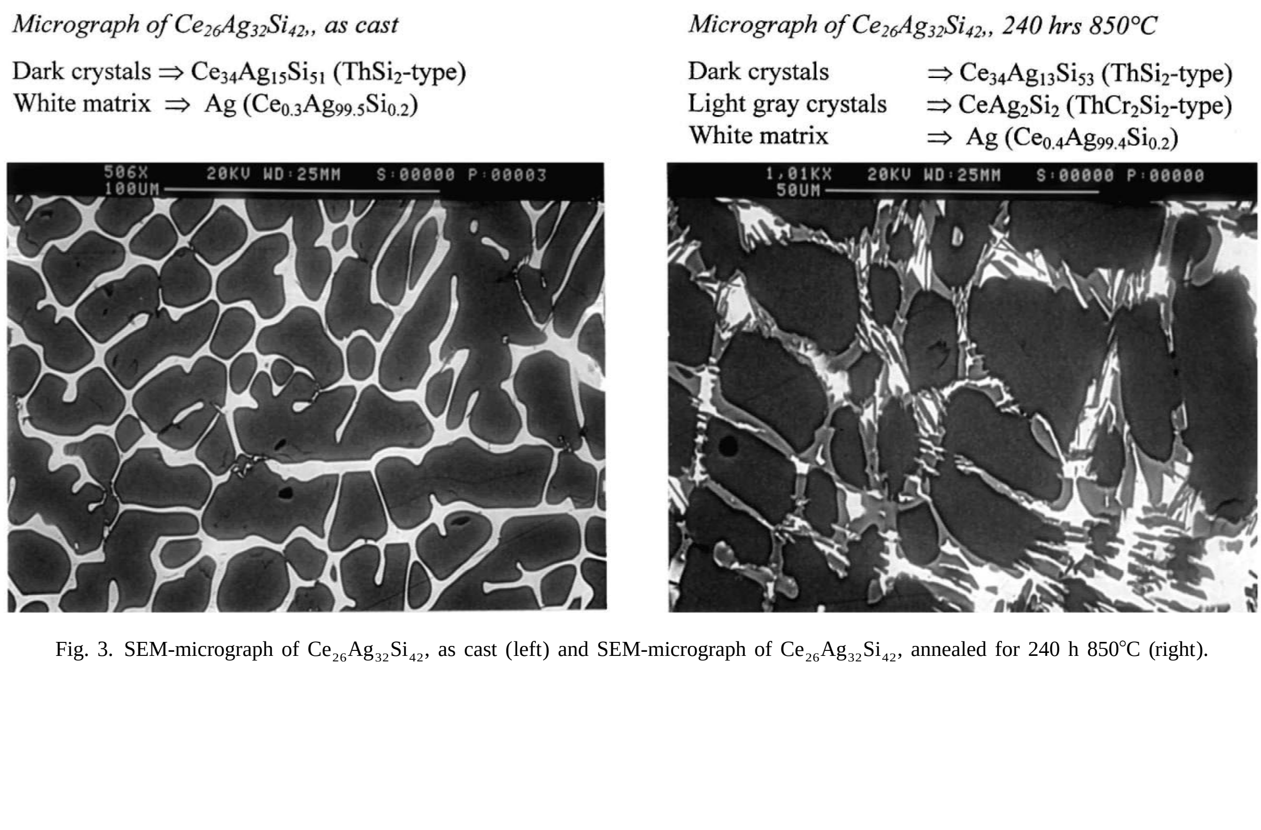

Fig. 3. SEM-micrograph of $Ce_{26}Ag_{32}Si_{42}$, as cast (left) and SEM-micrograph of $Ce_{26}Ag_{32}Si_{42}$, annealed for 240 h 850°C (right).

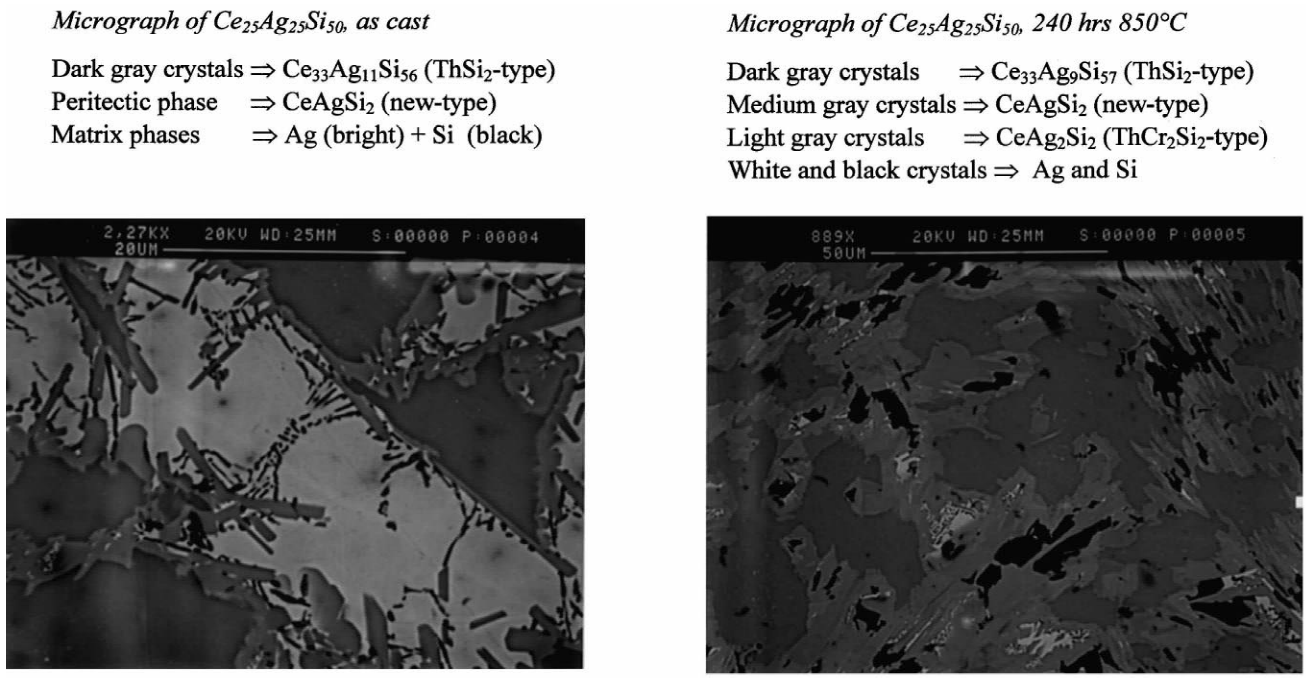

Fig. 4. SEM-micrograph of $Ce_{25}Ag_{25}Si_{50}$, as cast (left) and SEM-micrograph of $Ce_{25}Ag_{25}Si_{50}$, annealed for 240 h 850°C (right).

dependent preparation of the sample with $x_{Ag}=0.08$, $y=0.06$ also revealed antiferromagnetism below $T_N=5.7$ K, most likely due to a slight shift in the defect concentration (unaccounted for in EMPA measurements). For the latter two alloys a metamagnetic transition is observed at ~0.5 T (at 1.7 K), yielding a magnetic moment σ(5T) of ~0.85 μ_B (Fig. 10). The paramagnetic susceptibility for all the compositions studied (Fig. 6) exhibits a Curie–Weiss behaviour with the effective magnetic moment being close to the free Ce^{3+} ion value. The rather complex magnetic properties revealed in $Ce(Ag_xSi_{1-x})_{2-y}$ as a function of defect and atom substitution essentially reflects the puzzling behaviour observed in binary $CeSi_{2-y}$ [24,30–32].

$CeAg_2Si_2$ ($ThCr_2Si_2$–type): As shown in Fig. 13 (see also Table 2) the compound orders antiferromagnetically at $T_N=9.5$ K. A sharp increase in the susceptibility at low temperatures may reflect a complex incommensurate magnetic ordering proposed by [12] on the basis of powder neutron diffraction data.

In contrast, however, with the findings by [12] no

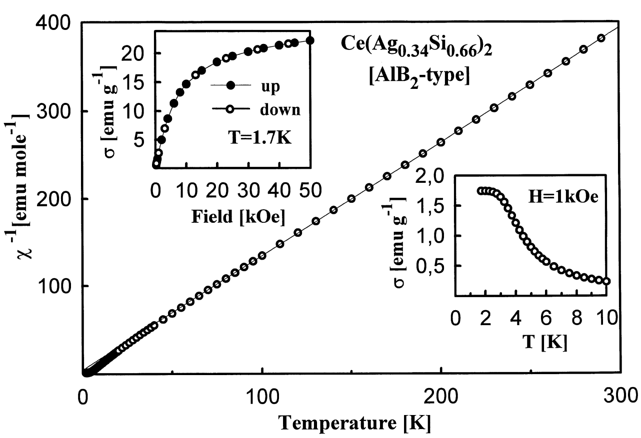

Fig. 5. Temperature variation of the inverse magnetic susceptibility for $CeAg_xSi_{2-x}$ [AlB_2-type]. The solid line is a fit of the experimental data to the Curie–Weiss law. The inset displays the magnetisation of this compound at low temperatures measured in 1 kOe.

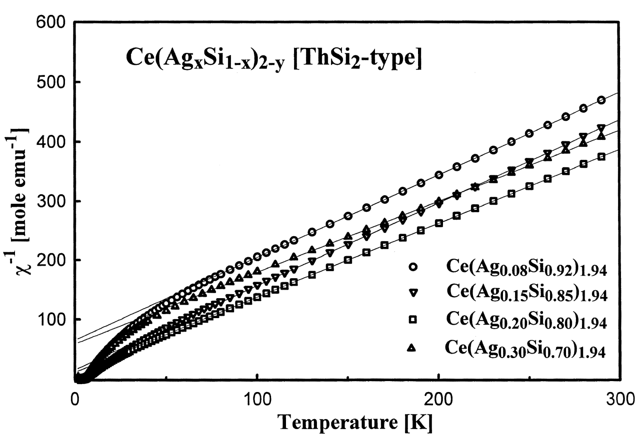

Fig. 6. Temperature variation of inverse magnetic susceptibility for the compounds of the ternary solid solution $Ce(Ag_xSi_{1-x})_{2-y}$ [$ThSi_2$-type] with $y=0.06$ at H = 1 kOe. The solid line is a fit of the experimental data to the Curie–Weiss law.

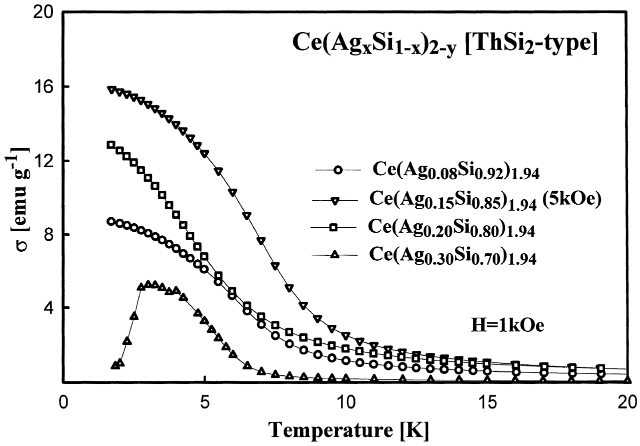

Fig. 7. Temperature variation of the magnetisation for the compounds of the ternary solid solution $Ce(Ag_xSi_{1-x})_{2-y}$ [$ThSi_2$-type] with $y=0.06$ measured at H=1 kOe.

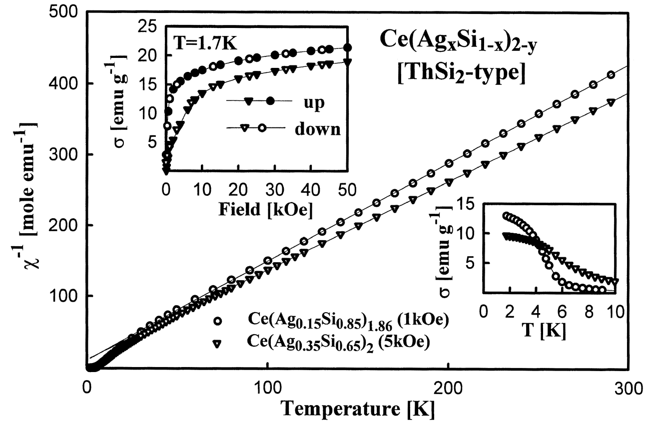

Fig. 9. Temperature variation of the inverse magnetic susceptibility for the ternary solid solution $Ce(Ag_xSi_{1-x})_{2-y}$ [$ThSi_2$-type] with $y=0.14$ and 0. The solid line is a fit of the experimental data to the Curie–Weiss law. The insets display the magnetisation of this compounds at low temperatures measured in 1 kOe and 5 kOe and the magnetisation versus applied field at 1.7 K.

ferromagnetic component is observed in the σ *v*s. *B* plot at 1.7 K (see the inset to Fig. 13). Above 150 K the susceptibility of $CeAg_2Si_2$ exhibits a Curie–Weiss behaviour with the parameters $\theta_p=-7$ K and $\mu_{eff}=2.42$ μ_B. A pronounced deviation from this law observed at lower temperatures is likely to reflect a thermal depopulation of crystal field levels.

$CeAgSi_2$ (unknown structure): The temperature dependence of the magnetisation (see Fig. 14) with characteristic irreversibility at low temperatures may suggest a ferromagnetic order which sets in below $T_C=7$ K. However, the magnitude of the magnetisation as well as the shape of the σ vs. *B* curves taken at 1.7 K indicate rather ferrimagnetic or canted antiferromagnetic behaviour. Above 100 K a Curie–Weiss law is observed with $\theta_p=-24$ K and $\mu_{eff}=2.13$ μ_B, whereas at lower temperatures χ^{-1}(T) deviates markedly from a straight line, presumably due to crystal field interaction.

Acknowledgements

This research has been sponsored by the FWF grant 8218 as part of a the EU-Human Capital and Mobility project ERBCHRX-CT93-0284. The authors are further-

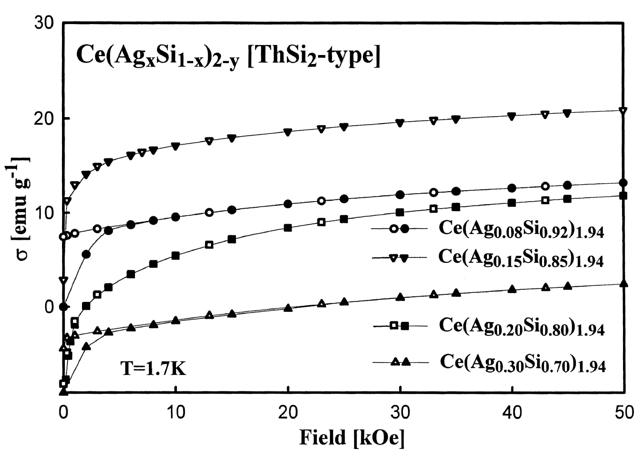

Fig. 8. Field dependence of the magnetisation with increasing field for the compounds of the ternary solid solution $Ce(Ag_xSi_{1-x})_{2-y}$ [$ThSi_2$-type] with $y=0.06$ measured at 1.7 K. The compounds with $x=0.2$ and 0.3 are shifted by an additional term of -10 emu$\cdot$g^{-1} in order to show the full curvature.

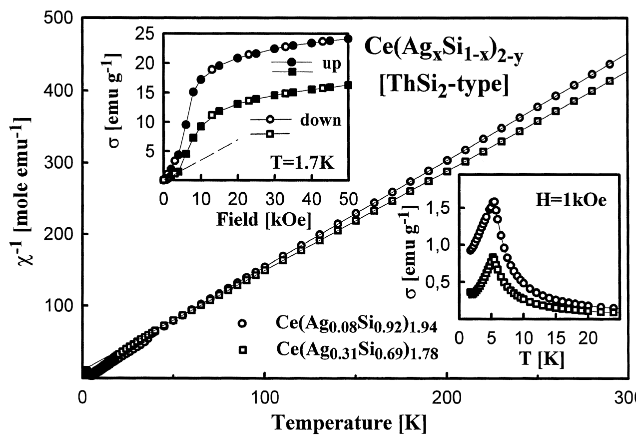

Fig. 10. Temperature variation of the inverse magnetic susceptibility for the antiferromagnetic compounds of the ternary solid solution $Ce(Ag_xSi_{1-x})_{2-y}$ [$ThSi_2$-type]. The solid line is a fit of the experimental data to the Curie–Weiss law. The insets display the magnetisation of this compounds at low temperatures measured in 1 kOe and the magnetisation versus applied field at 1.7 K.

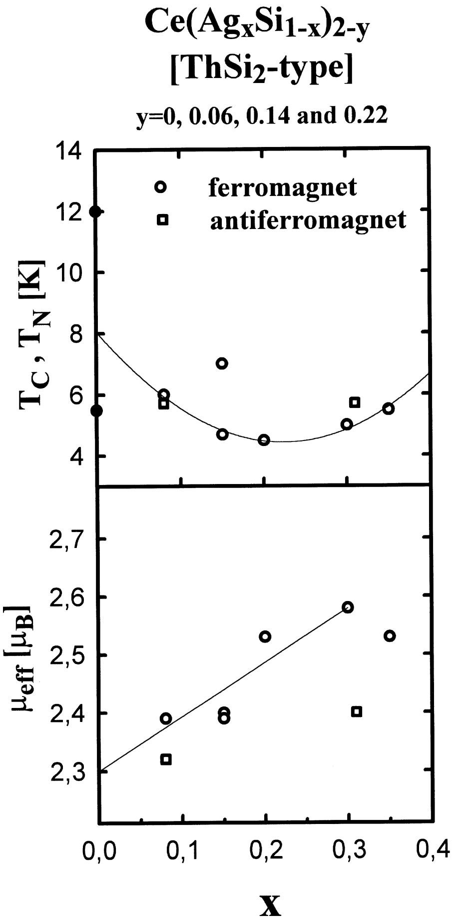

Fig. 11. Variation of T_C and μ_{eff} versus the content of Ag in the compounds of the ternary solid solution $Ce(Ag_xSi_{1-x})_{2-y}$ [$ThSi_2$-type].

more grateful to the Austrian–Italian and to the Austrian–Polish Scientific–Technological Exchange Program for fellowships in Genova, Wroclaw and Wien, respectively.

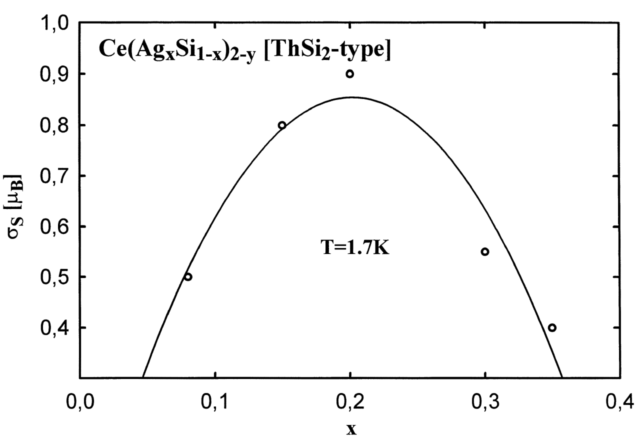

Fig. 12. Variation of the saturation moment σ_S versus the content of Ag in the compounds of the ternary solid solution $Ce(Ag_xSi_{1-x})_{2-y}$ [$ThSi_2$-type].

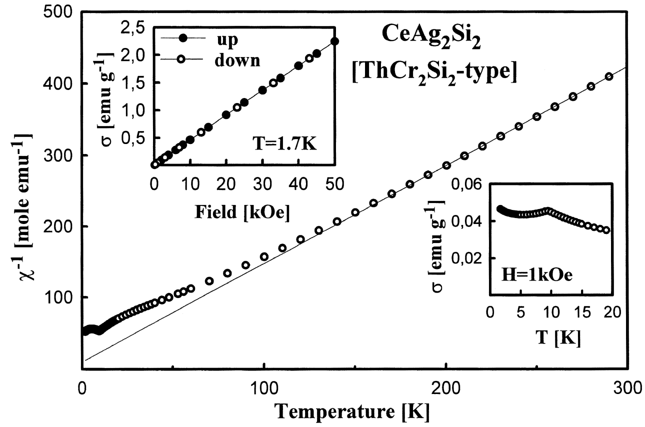

Fig. 13. Temperature variation of the inverse magnetic susceptibility for $CeAg_2Si_2$ [$ThCr_2Si_2$-type]. The solid line is a fit of the experimental data to the Curie–Weiss law. The inset displays the magnetisation of this compound at low temperatures measured in 1 kOe.

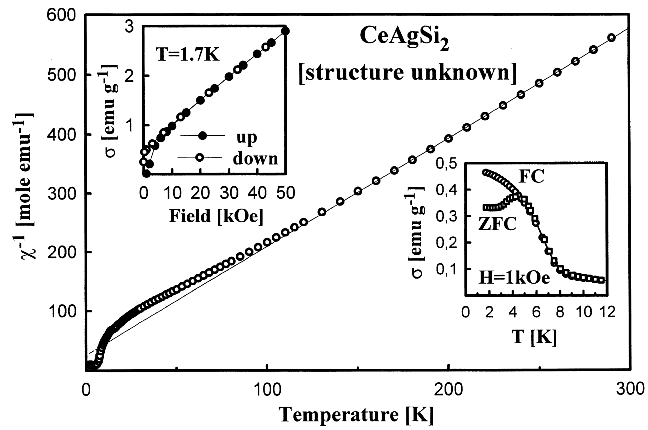

Fig. 14. Temperature variation of the inverse magnetic susceptibility for $CeAgSi_2$ [structure unknown]. The solid line is a fit of the experimental data to the Curie–Weiss law. The insets display the magnetisation of this compound at low temperatures measured in 1 kOe zero field cooled (ZFC) and field cooled (FC).

References

[1] L.A. Dvorina, T.S. Verkhoglyadova, in: Russian Metallurgy, Metally, Vol. 6, Izvestiya Akademii Nauk SSSR, 1996, p. 38, translated.
[2] H. Haschke, H. Nowotny, F. Benesovsky, Monatshefte für Chemie 97 (1966) 1453.
[3] G. Smith, A.G. Tharp, Q. Johnson, Acta Crystallogr. 22 (1967) 940.
[4] P. Duncumb, E.M. Jones, in: Tube Investments Company Report, Vol. 260, 1969.
[5] I. Mayer, I. Shidlovsky, Inorganic Chemistry 8 (6) (1969) 1240.
[6] I. Mayer, J. Cohen, J. Less-Common Met. 29 (1972) 221.
[7] I. Mayer, I. Felner, J. Less-Common Met. 29 (1972) 25.
[8] F. Steglich, J. Aarts, C.D. Bredl, W. Lieke, D. Meschede, W. Franz, H. Schäfer, Phys. Rev. Lett. 43 (25) (1979) 1892.
[9] E. Parthé, in: M. O'Keeffe, A. Navrotsky (Eds.), 2, Structure and Bonding in Crystals, Vol. 25, 1981, p. 256.
[10] K. Klepp, E. Parthé, Acta Crystallog. 38B (1982) 1105.
[11] G.Y.M. Al-Shaery, I.J. McColm, J. Less-Common Met. 98 (1984) L5.

[12] B.H. Grier, J.M. Lawrence, V. Murgai, R.D. Parks, Phys. Rev., Section B: Condensed Matter 29 (5) (1984) 2664.
[13] P. Rogl, in: K.A. Gschneidner Jr., L. Eyring (Eds.), Handbook on the Physics and Chemistry of Rare Earths, Vol. 7, North Holland, Amsterdam, 1984, pp. 1–264.
[14] I. Stapf, H. Jehn, J. Less-Common Met. 98 (1984) 173.
[15] K.A. Gschneidner Jr., F.W. Calderwood, Bull Alloy Phase Diag 6 (5) (1985) 439.
[16] A. Iandelli, J. Less-Common Met. 113 (1985) L25.
[17] H.L. Lukas, Silver–cerium–silicon, in: G. Petzow, G. Effenberg (Eds.), Ternary Alloys, Vol. 1, Verlag VCH, Weinheim, 1988, pp. 473–478.
[18] A. Munitz, A.B. Gokhale, G.J. Abaschian, Bull. Alloy Phase Diag. 10 (1989) 73.
[19] A. Szytula, J. Leciejewicz, in: K.A. Gschneidner Jr., L. Eyring (Eds.), Handbook on the Physics and Chemistry of Rare Earths, Vol. 12, North-Holland, Amsterdam, 1989, pp. 133–211.
[20] T.B. Massalski, P.R. Subramanian, H. Okamoto, L. Kacprzak, in: Binary Alloy Phase Diagrams, 2nd Ed, ASM International, Materials Park OH, USA, 1990.
[21] J. Rodriguez-Carvajal, FULLPROF: A Program for Rietveld Refinement and Pattern Matching Analysis, Abstracts of the Satellite Meeting on Powder Diffraction of the XV Congr. Intl. Union of Crystallogr., Talence, France, 1990, p. 127.
[22] J.G. Sereni, in: A. Gschneidner Jr., L. Eyring (Eds.), Handbook on the Physics and Chemistry of Rare Earths, Vol 15, North-Holland, Amsterdam, 1991, pp. 1–59.
[23] H.M. Murphy, K.U. Neumann, D. Visser, K.R.A. Ziebeck, Physica B 180/181 (1992) 601.
[24] J. Pierre, S. Auffret, B. Lambert-Andron, R. Madar, A.P. Murani, J.L. Soubeyroux, J. Magn. Magn. Mat. 104–107 (1992) 1207.
[25] P. Schobinger-Papamantellos, K.H.J. Buschow, J. Magn. Magn. Mat. 130 (1994) 242.
[26] P. Villars, A. Prince, H. Okamato, Handbook of Ternary Alloy Phase Diagrams, ASM International, Materials Park, OH, USA, 1995.
[27] G. Just, P. Paufler, J. Alloys Comp 232 (1996) 1.
[28] P. Boulet, D. Mazzone, H. Noël, P. Riani, P. Rogl, R. Ferro, Intermetallics 7 (1999) 931.
[29] E. Cordruwisch, D. Kaczorowski, A. Saccone, P. Rogl, R. Ferro, J. Phase Equilibria 200 (1999) 407.
[30] N. Sato, H. Mori, H. Yashima, T. Satoh, H. Takai, Solid State Commun. 51 (1984) 139.
[31] N. Sato, H. Mori, T. Satoh, T. Miura, H. Takai, J. Phys. Soc. Japan 57 (1988) 1384.
[32] J. Pierre, O. Laborde, E. Houssay, A. Rouault, J.P. Senateur, R. Madar, J. Phys.: Condensed Matter 2 (2) (1990) 431.
[33] M.M. Dzoba, I.A. Savysyuk, O.I. Shcherban, E.I. Gladyshevskii, Visnik Univ. Lviv., Ser. Khim. 36 (1996) 59.